J|A|C|S
ARTICLES
Published on Web 01/25/2006

Experimental and Computational Studies on the Mechanism of *N*-Heterocycle C−H Activation by Rh(I)

Sean H. Wiedemann,† Jared C. Lewis, Jonathan A. Ellman,* and Robert G. Bergman*

Contribution from the Department of Chemistry, University of California, and Division of Chemical Sciences, Lawrence Berkeley National Laboratory, Berkeley, California 94720

Received November 10, 2005; E-mail: rbergman@berkeley.edu

Abstract: Evidence is presented for a proposed mechanism of C−H activation of 3-methyl-3,4-dihydroquinazoline (**1**) by $(PCy_3)_2RhCl$. One intermediate (**3**), a coordination complex of **1** with $(PCy_3)_2RhCl$, was identified along the path to the Rh-*N*-heterocyclic carbene product of this reaction (**2**). Isotopic labeling and reaction-rate studies were used to demonstrate that C−H activation takes place intramolecularly on the reaction coordinate between **3** and **2**. Computational studies corroborate the proposed mechanism and suggest that the rate-limiting step is oxidative addition of the C−H bond to the metal center. The consequences of this mechanism for coupling reactions of *N*-heterocycles that occur via Rh-catalyzed C−H bond activation are discussed.

Introduction

Our group[1] and others[2] have been interested in the use of directing groups to promote and control regioselectivity in catalytic C−H additions to olefins. Murai and co-workers' method for Ru-catalyzed *ortho*-alkylation of acetophenones was the first general application of directed C−H activation toward C−C bond formation.[3] Mechanistic studies carried out on that system showed that the keto group functions by coordinating to the catalyst and establishing a geometry that facilitates cyclometalation.[4,5] Using mechanistic insight, the scope of competent directing groups was expanded to include many other functional groups that can act as Ru^0 ligands.[6]

Contemporaneously with these investigations, it was revealed that a single atom, the ring heteroatom of an *N*-heterocycle, can perform the same function as a pendant directing group, promoting selective functionalization of an adjacent C−H bond. Because predictable methods for heterocycle elaboration are critical to the synthesis of pharmaceuticals, there is great potential benefit in understanding the mechanistic pathways unique to this substrate class. The first example of a direct catalytic coupling between a heterocycle and an olefin was reported by Jordan and co-workers in 1989.[7] Using a zirconocene catalyst, the C6−H bond of 2-picoline was added to propene in high yield. Despite a thorough investigation of that reaction's mechanism, its substrate scope could not be significantly enlarged.[8] In 1992, Moore and co-workers reported heterocycle/olefin coupling with the incorporation of CO.[9] The development of this reaction by other investigators led to limited gains in terms of scope and utility; direct mechanistic information remains scarce because metal−carbonyl clusters are probable intermediates.[10]

Olefin/heterocycle coupling has made a resurgence recently with the advent of potent electrophilic catalysts. Coupling reactions targeting electronically activated C−H bonds of indole, for example, have been demonstrated for Ru,[11] Pt,[12] and an organo-catalyst.[13] Still, the direct coupling of diverse and cheap α-olefins to minimally activated heterocycles remains a tantalizingly underdeveloped transformation.[14]

† Present address: Graduate School of Pharmaceutical Sciences, University of Tokyo, Hongo 7-3-1, Bunkyo-ku, Tokyo 113-0033, Japan.

(1) Wiedemann, S. H.; Bergman, R. G.; Ellman, J. A. In *Handbook of C−H Transformations*; Dyker, G., Ed.; Wiley-VCH: Weinheim, 2005; Vol. 1, p 187.
(2) (a) Guari, Y.; Sabo-Etienne, S.; Chaudret, B. *Eur. J. Inorg. Chem.* **1999**, 1047. (b) Ritleng, V.; Sirlin, C.; Pfeffer, M. *Chem. Rev.* **2002**, *102*, 1731. (c) Kakiuchi, F.; Murai, S. In *Activation of Unreactive Bonds in Organic Synthesis*; Murai, S., Ed.; Freund Pub. House: London, 1999; Vol. 3, p 47.
(3) Murai, S.; Kakiuchi, F.; Sekine, S.; Tanaka, Y.; Kamatani, A.; Sonoda, M.; Chatani, N. *Nature* **1993**, *366*, 529.
(4) For a discussion of a cyclometalation mechanism involving direct oxidative addition, see: Kakiuchi, F.; Sekine, S.; Tanaka, Y.; Kamatani, A.; Sonoda, M.; Chatani, N.; Murai, S. *Bull. Chem. Soc. Jpn.* **1995**, *68*, 62.
(5) For a discussion of a cyclometalation mechanism involving conjugate addition of Ru^0, followed by α-elimination, see: (a) Matsubara, T.; Koga, N.; Musaev, D. G.; Morokuma, K. *J. Am. Chem. Soc.* **1998**, *120*, 12692. (b) Matsubara, T.; Koga, N.; Musaev, D. G.; Morokuma, K. *Organometallics* **2000**, *19*, 2318.
(6) Kakiuchi, F.; Murai, S. *Acc. Chem. Res.* **2002**, *35*, 826.
(7) Jordan, R. F.; Taylor, D. F. *J. Am. Chem. Soc.* **1989**, *111*, 778.
(8) Jordan, R. F.; Taylor, D. F.; Baenziger, N. C. *Organometallics* **1990**, *9*, 1546.
(9) Moore, E. J.; Pretzer, W. R.; O'Connell, T. J.; Harris, J.; Labounty, L.; Chou, L.; Grimmer, S. S. *J. Am. Chem. Soc.* **1992**, *114*, 5888.
(10) (a) Chatani, N.; Fukuyama, T.; Kakiuchi, F.; Murai, S. *J. Am. Chem. Soc.* **1996**, *118*, 493. (b) Fukuyama, T.; Chatani, N.; Tatsumi, J.; Kakiuchi, F.; Murai, S. *J. Am. Chem. Soc.* **1998**, *120*, 11522. (c) Chatani, N.; Fukuyama, T.; Tatamidani, H.; Kakiuchi, F.; Murai, S. *J. Org. Chem.* **2000**, *65*, 4039. (d) Szewczyk, J. W.; Zuckerman, R. L.; Bergman, R. G.; Ellman, J. A. *Angew. Chem., Int. Ed.* **2001**, *40*, 216.
(11) (a) Youn, S. W.; Pastine, S. J.; Sames, D. *Org. Lett.* **2004**, *6*, 581. (b) Pittard, K. A.; Lee, J. P.; Cundari, T. R.; Gunnoe, T. B.; Petersen, J. L. *Organometallics* **2004**, *23*, 5514.
(12) (a) Liu, C.; Han, X.; Wang, X.; Widenhoefer, R. A. *J. Am. Chem. Soc.* **2004**, *126*, 3700. (b) Liu, C.; Widenhoefer, R. A. *J. Am. Chem. Soc.* **2004**, *126*, 10250. (c) Liu, C.; Han, X. Q.; Wang, X.; Widenhoefer, R. A. *J. Am. Chem. Soc.* **2004**, *126*, 10493.
(13) (a) Paras, N. A.; MacMillan, D. W. C. *J. Am. Chem. Soc.* **2001**, *123*, 4370. (b) Austin, J. F.; MacMillan, D. W. C. *J. Am. Chem. Soc.* **2002**, *124*, 1172.

10.1021/ja0576684 CCC: $33.50

Scheme 1. The Proposed Mechanism for Rhodium-Catalyzed Benzimidazole/Alkene Coupling

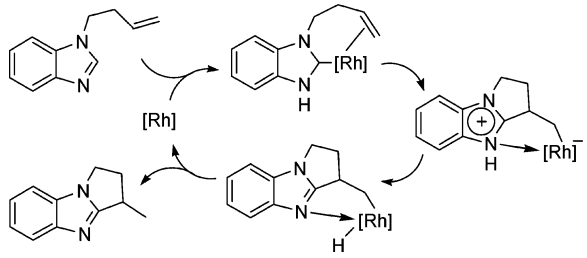

In 2001, we described a Rh(I)/phosphine catalyst system capable of promoting the C−H coupling of *N*-heterocycles to olefins.[15] Initially, azoles and benzazoles were shown to be efficiently activated.[15a] The substrate specificity of this reaction was illuminated by a mechanistic study of one benzimidazole derivative.[15b] Remarkably, in the principal catalyst resting state, the benzimidazole substrate has undergone rearrangement, the resulting product binding to rhodium as an *N*-heterocyclic carbene (NHC) ligand.

With a Rh−NHC complex as the starting point, rate studies and DFT calculations were carried out and used as the basis for a proposed mechanism of Rh-catalyzed heterocycle/alkene coupling (Scheme 1). Subsequent reaction development focused on heterocycles capable of forming and stabilizing an NHC tautomer, and the substrate scope of Rh-catalyzed olefin coupling was expanded to include azolines[16] and, more recently, dihydroquinazolines[17] (eq 1).

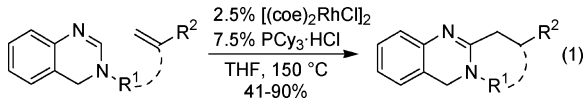

Yet, portions of the proposed mechanism were still not fully understood. In fact, the most remarkable step, the formation of a Rh−NHC complex from heterocycle and Rh(I) via H-migration, is without literature precedent. Being a unique C−H bond activation process and a mild method for the preparation of NHC ligands, we felt that a deeper understanding of this fundamental transformation could lead to new opportunities for reaction discovery. The results of experimental and computational studies of Rh(I)-mediated heterocycle C−H activation reactions are described in this report. On the basis of these studies, a detailed mechanism for C−H activation is presented and evaluated in the context of catalysis.

Results

Structural Studies. Following some initial work, 3-methyl-3,4-dihydroquinazoline (**1**) was chosen from among the heterocycles active toward Rh-catalyzed C−H functionalization as our platform for mechanistic study. It reacted cleanly with stoichiometric amounts of the catalyst mixture used in olefin coupling reactions, $[(coe)_2RhCl]_2/PCy_3$ (coe = *cis*-cyclooctene, Cy = cyclohexyl), to give carbene complex **2** (eq 2).[18] These conditions were previously used to synthesize an analogous NHC-complex from *N*-methylbenzimidazole.[19] As in that case, the structure of **2** was elucidated by single-crystal X-ray analysis (Figure 1).

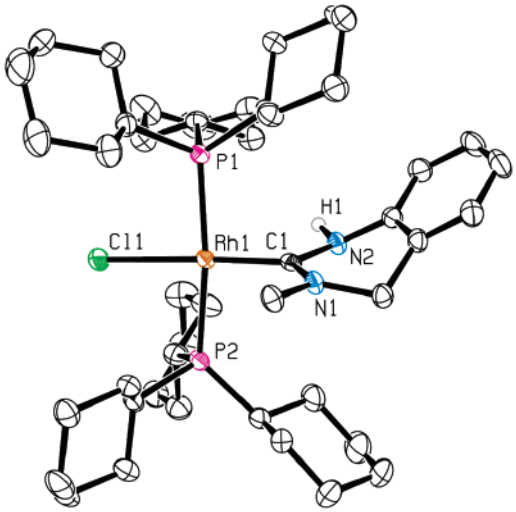

Figure 1. X-ray crystal structure (ORTEP diagram) of **2**.

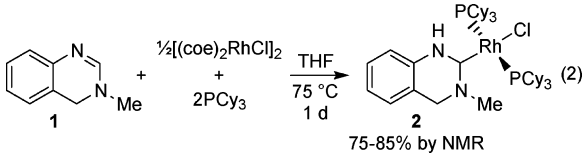

The irreversible conversion of **1** to **2** occurs between 45 and 75 °C, well below the temperature required for olefin coupling (150 °C). At temperatures below 35 °C, carbene formation is sluggish and an orange precipitate forms over 1−3 d. Based on ^{1}H and ^{31}P NMR analysis, this precipitate (**3**) was found to be a new Rh-complex of **1**. Further in situ NMR study of carbene formation reactions revealed the presence of **3** at a variety of temperatures. Importantly, throughout all reactions, the mass balance of added **1** could be accounted for as either free **1**, carbene **2**, or complex **3**.

The structure of **3** was assigned to be a *trans*-2:1 PCy_3/**1** coordination complex of Rh(I)Cl based on peak integration in ^{1}H NMR spectra and peak splitting in ^{31}P NMR spectra. Single-crystal X-ray analysis of **3** was not possible because, regardless of solvent system, **3** crystallized with too much interstitial solvent to survive even gentle handling. NMR studies of isotopically labeled materials, on the other hand, did provide details about the solution structure of **3**. Using a convergent three-step procedure, ^{15}N1-**1** was prepared from ^{15}N-benzamide and used to synthesize ^{15}N1-**3** (Scheme 2). The magnitude of ^{15}N−^{31}P coupling observed in the ^{31}P spectrum of ^{15}N1-**3** was consistent with a Rh(I) complex bearing ^{15}N-heteroarene and phosphine ligands in a cis orientation (3.0 Hz).[20] Given this

(14) Some oxidative protocols for the heterocycle/olefin couple have appeared recently: (a) DeBoef, B.; Pastine, S. J.; Sames, D. *J. Am. Chem. Soc.* **2004**, *126*, 6556. (b) Yi, C. S.; Yun, S. Y.; Guzei, I. A. *Organometallics* **2004**, *23*, 5392. (c) Beccalli, E. M.; Broggini, G. *Tetrahedron Lett.* **2003**, *44*, 1919. (d) Ferreira, E. M.; Stoltz, B. M. *J. Am. Chem. Soc.* **2003**, *125*, 9578.

(15) (a) Tan, K. L.; Bergman, R. G.; Ellman, J. A. *J. Am. Chem. Soc.* **2001**, *123*, 2685. (b) Tan, K. L.; Bergman, R. G.; Ellman, J. A. *J. Am. Chem. Soc.* **2002**, *124*, 13964. (c) Tan, K. L.; Bergman, R. G.; Ellman, J. A. *J. Am. Chem. Soc.* **2002**, *124*, 3202. (d) Tan, K. L.; Vasudevan, A.; Bergman, R. G.; Ellman, J. A.; Souers, A. J. *Org. Lett.* **2003**, *5*, 2131. (e) Tan, K. L.; Park, S.; Ellman, J. A.; Bergman, R. G. *J. Org. Chem.* **2004**, *69*, 7329.

(16) Wiedemann, S. H.; Bergman, R. G.; Ellman, J. A. *Org. Lett.* **2004**, *6*, 1685.

(17) Wiedemann, S. H.; Ellman, J. A.; Bergman, R. G. *J. Org. Chem.* In press.

(18) For a previous synthesis of a **1**-derived M−NHC complex, see: Basato, M.; Benetollo, F.; Facchin, G.; Michelin, R. A.; Mozzon, M.; Pugliese, S.; Sgarbossa, P.; Sbovata, S. M.; Tassan, A. *J. Organomet. Chem.* **2004**, *689*, 454.

(19) Lewis, J. C.; Wiedemann, S. H.; Bergman, R. G.; Ellman, J. A. *Org. Lett.* **2004**, *6*, 35.

(20) Carlton, L.; De Sousa, G. *Polyhedron* **1993**, *12*, 1377.

Scheme 2. Synthesis of Isotopically Labeled Rh-Complexes

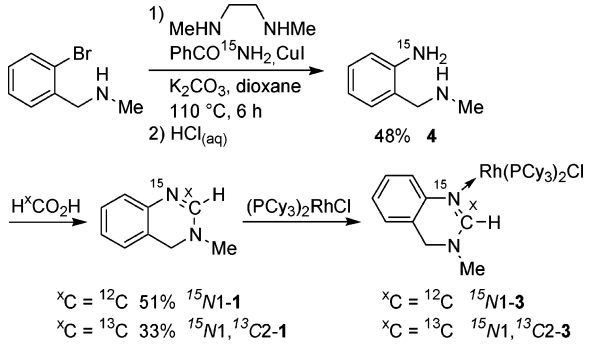

strong evidence that **1** binds to rhodium through N1, rather than N3, we proposed the structure of **3** depicted in Scheme 2.

To confirm that the heterocycle was indeed σ-bound to rhodium, we synthesized and formed the Rh(I)-complex of $^{15}N1,^{13}C2$-**1** (Scheme 2). The ^{13}C chemical shift change of the amidine carbon upon complexation was found to be small and upfield ($\Delta\delta = +5.1$ ppm). Gladysz and others have shown that small chemical shift changes are expected for σ-complexes of carbonyls to electron-rich late metals, whereas large downfield shift changes ($\Delta\delta = -90$ to 140 ppm) are observed for the corresponding π-complexes.[21]

With confirmation of σ-bonding in **3** in hand, DFT calculations were performed on a model system (using PMe_3 in place of PCy_3, **5**) to obtain more detailed structural information. After energy minimization, **5** adopted a calculated geometry that can be described as an intersection of two orthogonal molecular planes, where one plane is made up of the dihydroquinazoline framework and the other is defined by the Rh-square plane (Figure 2).[22] In this conformation, the C8−H atom of bound **1**

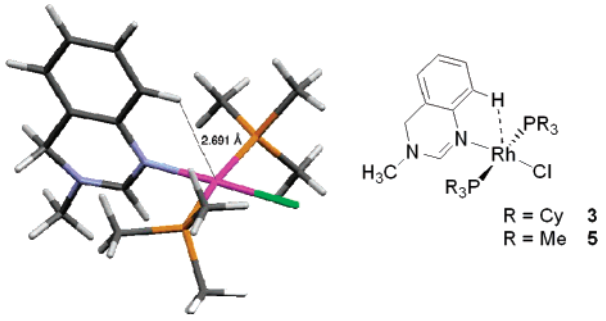

Figure 2. Calculated structure for **5** showing the Rh−H "pre-agostic" interaction.

resides 2.7 Å above the square-planar rhodium center. At that distance, the M−H close contact falls into the upper range of "pre-agostic" interactions.[23] If the true geometry of **3** in solution were analogous to the calculated geometry of **5** in the gas phase, then the resulting pre-agostic interaction would cause the ^{1}H NMR resonance for C8−H to be strongly shifted downfield. Indeed, upon complexation of **1** to $(PCy_3)_2$RhCl, a single Ar−H resonance attributable to C8-H was observed 3 ppm downfield

Scheme 3. Possible Mechanisms for Carbene Formation via C−H Activation

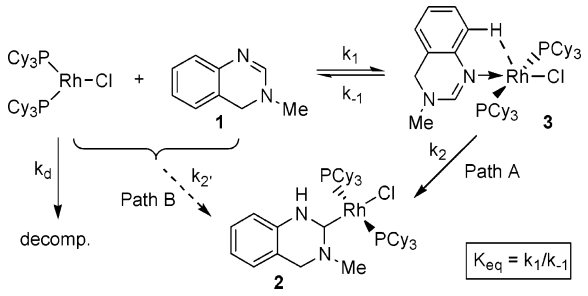

of the others ($\delta = 10$ vs 6.9 ppm), supporting the structure of **3** depicted in Figure 2.[24]

Reactivity Studies. Before proceeding further, it became necessary to ascertain the role of **3** in the formation of **2**. Two C−H activation reactions were monitored concurrently at 60 °C: one starting from isolated **3**, and the other starting from **1** and $[(coe)_2RhCl]_2/2PCy_3$. In both of these reactions, an observable equilibrium between **1** and **3** was rapidly established. From this maximum point, the concentration of **3** dropped continuously to zero as **1** was consumed to form **2**. Thus, either **3** is a reactive intermediate lying on the path to **2** (Scheme 3, path A), or the equilibrium between **1** and **3** is a kinetic "dead end", with C−H activation arising from a separate bimolecular pathway (Scheme 3, path B).

This sort of uncertainty is typically resolved by comparing the rate that product is formed by the reaction of starting materials to the rate that product is formed by subjecting the isolated intermediate to the same reaction conditions. Unfortunately, that exact experiment is not possible in the present case, because it relies on k_1/k_{-1} equilibration being sufficiently slow. At the temperatures required to dissolve **3** for NMR reaction analysis (>45 °C), there is rapid equilibration between **1** and **3**. Once equilibrium is established, path A and path B become kinetically indistinguishable; by applying the equilibrium approximation, the rate expression for either path can be rewritten so that it differs from the rate expression for the other path only in the way that k_{obs} is defined (eq 3).

$$\mathrm{d}[\mathbf{2}]/\mathrm{d}t\ (\text{path A}) = k_2[\mathbf{3}] \tag{3a}$$

$$\mathrm{d}[\mathbf{2}]/\mathrm{d}t\ (\text{path B}) = k_{2'}[\mathbf{1}][(PCy_3)_2RhCl] \tag{3b}$$

$$K_{eq} = [\mathbf{3}]/([\mathbf{1}][(PCy_3)_2RhCl]) \tag{3c}$$

$$\mathrm{d}[\mathbf{2}]/\mathrm{d}t\ (\text{path B}) = (k_{2'}/K_{eq})[\mathbf{3}] = k_{obs}[\mathbf{3}] = k_2[\mathbf{3}] = \mathrm{d}[\mathbf{2}]/\mathrm{d}t\ (\text{path A}) \tag{3d}$$

Eventually, the two reaction paths were discriminated by monitoring a reaction between **1**, $[(coe)_2RhCl]_2$, and PCy_3 at a temperature low enough for **1** and **3** to slowly approach equilibrium, yet high enough for the rate of formation of **2** (d[**2**]/dt) to be accurately measured. Accordingly, at 37 °C the concentrations of **1**, **2**, and **3** were measured continuously as a function of time using in situ ^{1}H NMR analysis (Figure 3). If

(21) (a) Mendez, N. Q.; Seyler, J. W.; Arif, A. M.; Gladysz, J. A. *J. Am. Chem. Soc.* **1993**, *115*, 2323. (b) Stark, G. A.; Gladysz, J. A. *Inorg. Chem.* **1996**, *35*, 5509.

(22) While we have chosen to depict the metal center of **3** as square planar, we cannot rule out the presence of one weakly bound inner-sphere solvent ligand.

(23) Yao, W. B.; Eisenstein, O.; Crabtree, R. H. *Inorg. Chim. Acta* **1997**, *254*, 105.

(24) Pre-agostic interactions have been identified as intermediates preceding C−H oxidative addition. The question of whether the C8−H bond of **3** can undergo metal-insertion is beyond the scope of this report. For a discussion of this rare type of interaction in a related system, see: Lewis, J. C.; Wu, J.; Bergman, R. G.; Ellman, J. A. *Organometallics* **2005**, *24*, 5737.

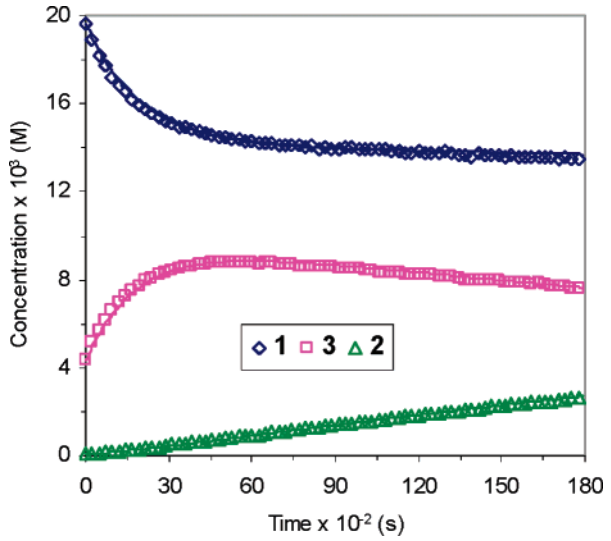

Figure 3. Plot of concentration versus time for the species present during the reaction of **1** with Rh(I)/PCy$_3$ at 36.7 °C. The solid curves depict kinetics simulations of the data (path A: $k_1 = (1.0 \pm 0.2) \times 10^{-2}$ M^{-1} s^{-1}, $k_{-1} = (2.0 \pm 0.2) \times 10^{-4}$ s^{-1}, $k_d = (1.10 \pm 0.05) \times 10^{-5}$ s^{-1}).

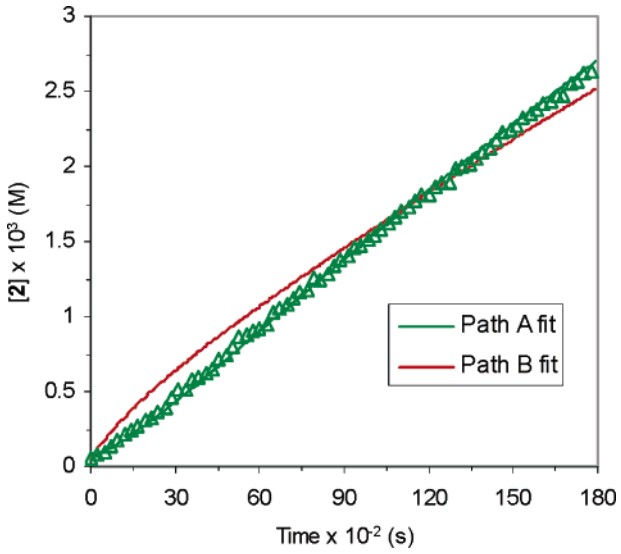

Figure 4. Plot of [**2**] versus time from Figure 3, enlarged to show fits for two possible reaction pathways depicted in Scheme 3 (path A: $k_2 = (1.809 \pm 0.003) \times 10^{-5}$ s^{-1}).

path A were operative, d[**2**]/d*t* would be expected to increase over time as [**3**] increases, resulting in an upward curving graph of [**2**] versus time. In contrast, path B predicts that as [**1**] and [(PCy$_3$)$_2$RhCl] are depleted to form **3**, d[**2**]/d*t* should decrease, resulting in a downward curving graph of [**2**] versus time. The observed plot of [**2**] versus time showed slight upward curvature at early conversion, when the approach to equilibrium was most rapid, providing support for path A over path B (Figure 4). To further confirm this qualitative result, the observed concentration versus time profiles were fitted to the mechanistic pathways illustrated in Scheme 3 with the aid of the Gepasi kinetics modeling program.[25] The simulated [**2**] versus time profile generated from path A matched experimental data far better than the profile derived from path B (Figure 4).

Given that **3** is an intermediate on the pathway to **2**, and has the same stoichiometry as **2**, the simplest plausible mechanism for C−H activation would seem to be intramolecular H-transfer.

Scheme 4. Proposed Mechanism for Isotopic Scrambling of *C2-D*-**3**

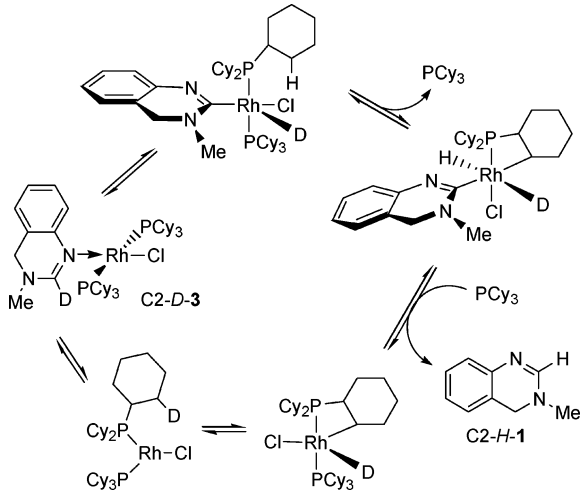

Such a mechanism would lead to a first-order dependence of d[**2**]/d*t* on the concentration of **3**. The simulated reaction profiles generated for path A by kinetics modeling software (Figure 3, smooth curves) presuppose first-order dependence on **3** and precisely fit observed data. While this does constitute evidence in favor of an intramolecular mechanism, goodness of fit is generally regarded as a weak measure of reaction order. We posed two crucial questions, therefore, to clarify the role of bimolecular processes in the seemingly intramolecular conversion of **3** to **2** via path A: (1) Is the H removed from C2 the same atom as that added to N1? (2) If so, does that H exchange with any others as it is transferred? A deuterium tracer experiment was performed to shed light on these questions.

C2-D-**1** reacted with the usual Rh(I)/PCy$_3$ mixture to produce *N1-D*-**2** with 88% isotopic incorporation at the N1 position (eq 4). Some minor deuterium loss can be explained by invoking transient Rh−D intermediates. If such intermediates underwent reversible cyclometalation, a well-known process for Rh(I)/PCy$_3$ complexes,[26] deuterium exchange into phosphine cyclohexyl groups could occur (Scheme 4). Because rhodium hydride intermediates were indeed located computationally (vida infra) and a reaction pathway involving the dissociation of PCy$_3$ was recognized experimentally (vida infra), this mechanism seems reasonable. Moreover, the extent of deuterium loss is small and thus does not jeopardize the conclusion that the C2−H of **1** is the primary source of N1−H in **2**.[27]

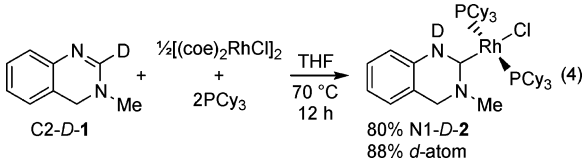

In an effort to answer the question of whether H-transfer from C2 to N1 occurs directly or with intermolecular exchange, a double-labeling crossover experiment was carried out using equal amounts of *C2-D*-**1** and ^{15}*N1*-**1** (Table 1). The amount of

(25) (a) Mendes, P. *Comput. Appl. Biosci.* **1993**, *9*, 563. (b) Mendes, P. *Trends Biochem. Sci.* **1997**, *22*, 361. (c) Mendes, P.; Kell, D. B. *Bioinformatics* **1998**, *14*, 869.

(26) Cyclometalation into the alkyl groups of (PCy$_3$)$_2$RhCl has been implicated in the decomposition of this complex: Hietkamp, S.; Stufkens, D. J.; Vrieze, K. *J. Organomet. Chem.* **1978**, *152*, 347.

Table 1. Double Labeling Crossover Experiment Data

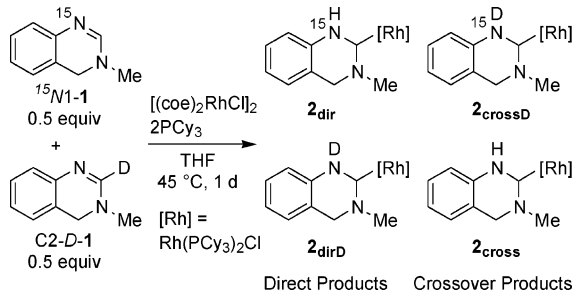

	% yield				% crossover
time (h:min)	$\mathbf{2}_{dir}$	$\mathbf{2}_{cross}$	$\mathbf{2}_{dirD} + \mathbf{2}_{crossD}$[a]	total	observed[b]
0:00	0	0	0	0	NA
1:30	10	1	6	16	5
4:30	24	1	14	39	4
8:20	34	3	19	56	5
21:10	41	5	26	72	7
27:20	41	6	27	75	8

[a] $\mathbf{2}_{dirD}$ and $\mathbf{2}_{crossD}$ are not independently observable by ^{1}H NMR analysis. [b] Observed % crossover = % $\mathbf{2}_{cross}$/% total. Because $\mathbf{2}_{crossD}$ is not independently observable, the true extent of isotopic scrambling may be greater than the observed value.

observable crossover product (^{14}*N*1-*H*-**2**, $\mathbf{2}_{cross}$) produced in this experiment was no greater than the amount expected to arise from minor deuterium loss via the pathway discussed above. Furthermore, the fact that percent crossover stayed nearly constant at first, and then slowly rose over long reaction times, suggests that some of the observed crossover product may have arisen from isotopic scrambling between NHC products after they were formed. Hence, we conclude that the conversion of **3** to **2** results from intramolecular H-transfer,[28] and we rule out mechanisms involving the exchange of hydrides between metal centers or the reductive elimination and recapture of hydrides as HCl.[29]

Rate Studies. Assuming that C−H activation takes place via intramolecular H-transfer, according to the mechanism presented in path A of Scheme 3, an overall rate law can be derived for the conversion of **1** to **2** (eq 5). By applying this expression, d[**2**]/d*t* and the concentrations of **1** and $(PCy_3)_2$RhCl can be used to calculate k_2, which provides information about the C−H activation step in isolation. Unfortunately, it is difficult to ascertain the concentration of $(PCy_3)_2$RhCl necessary for this calculation because (1) $(PCy_3)_2$RhCl lacks diagnostic resonances for quantification by ^{1}H NMR, (2) it exists in equilibrium with its dimer and other complexes (Scheme 5),[30] and (3) it undergoes decomposition over the course of the carbene formation reaction.[31] In addition to causing uncertainty in the concentration of "active Rh", the tendency of $(PCy_3)_2$RhCl toward decomposition readily explains the observed reaction yields of not greater than 85% for 1:1 reactions between **1** and Rh(I)/PCy_3.[32] Thus, to compute k_2 given the three quantities measurable by ^{1}H NMR analysis ([**1**], [**3**], [**2**]), kinetics simulation software was used. By allowing the software to freely vary $[(PCy_3)_2RhCl]$ and the rate constants defined in path A of Scheme 3, good fits to empirical data were achieved (relative errors for k_2 < 1%).[33]

Scheme 5. Equilibria Governing $[(PCy_3)_2RhCl]$

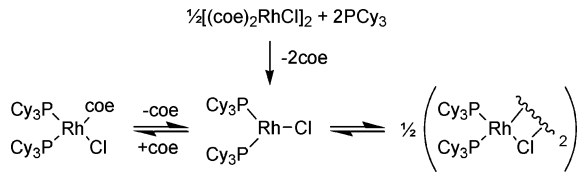

$$d[\mathbf{2}]/dt = k_2[\mathbf{3}] = K_{eq}k_2[\mathbf{1}][(PCy_3)_2RhCl] \qquad (5)$$

To obtain activation parameters for C−H activation, a series of reactions, starting from isolated **3**, were monitored continuously by in situ ^{1}H NMR analysis over a range of temperatures (45−75 °C). In addition to values for k_2, kinetics simulations provided values for K_{eq}. From these values, a Van't Hoff plot was constructed and fitted to a linear function (Figure S-1c). Probably as a result of the aforementioned uncertainty in $[(PCy_3)_2RhCl]$, there was considerable scatter of data about the best-fit Van't Hoff line ($r^2 = 0.82$). Nevertheless, the slope and intercept of the fitting function did correspond to thermodynamic parameters that are consistent with reversible binding of a neutral ligand ($\Delta H° = -5.9 \pm 0.8$ kcal/mol and $\Delta S° = -10 \pm 2$ cal/mol·K).

Initially, when data collected for k_2 were transformed into an Eyring plot, deviation from linear behavior was once again observed. This imprecision was puzzling to us because the parameters governing k_2, [**2**] and [**3**], are accurately measurable. In an effort to trace the source of what seemed to be systematic error, we hypothesized that C−H activation might proceed through a rate-limiting transition structure with only one bound PCy_3. In such a sequence, rapid, post-rate-limiting recoordination of free PCy_3 would complete the conversion to **2** (eq 6). This mechanism predicts an inverse dependence of d[**2**]/d*t* on [free PCy_3]. Systematic error would thus occur if small but differing amounts of free PCy_3 were introduced, for example, from different batches of reaction starting material (**3**).

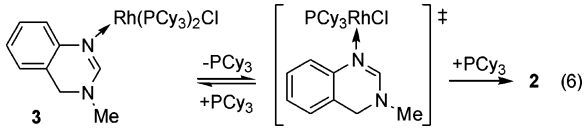

In agreement with our hypothesis, we found that a small amount of added PCy_3 (13 mM = 0.5 equiv vs $[Rh]_t$) generally did lead to a 2−2.5-fold reduction in the rate of carbene formation. However, for [free PCy_3] > 13 mM, the rate of carbene formation was found to be independent of [PCy_3] (Figure 5). Taken together, these data reveal the existence of two competing reaction pathways between **3** and **2**: one that is dissociative in phosphine and one that is not.

(27) The ^{1}H NMR signals of PCy_3 are too poorly resolved to permit the measurement of any minor deuterium incorporation there. Also, *N*1-*D*-**2** is not soluble enough for the same measurement to be made by ^{2}H NMR.
(28) Another scenario that is consistent with the observed data is a large extent of crossover in conjunction with a large kinetic isotope effect. This interpretation is invalidated by the small measured kinetic isotope effect (vide infra).
(29) Other evidence that free HCl is uninvolved in C−H activation is provided by our observation that the rate of formation of **2** is insensitive to added acid (HCl) or base (K_2CO_3).
(30) (a) Van Gaal, H. L. M.; Van Den Bekerom, F. L. A. *J. Organomet. Chem.* **1977**, *134*, 237. (b) Van Gaal, H. L. M.; Moers, F. G.; Steggerda, J. J. *J. Organomet. Chem.* **1974**, *65*, C43.
(31) For a description of the decomposition of $(PCy_3)_2$RhCl, see ref 30a.
(32) Incomplete conversion of **1** was also observed for reactions employing related trialkylphosphines ($PiPr_3$, $PtBu_2Me$). Higher conversions can be obtained by using excess $(PR_3)_2$RhCl.
(33) The omission of more complicated [Rh] equilibria was not found to affect data fitting.

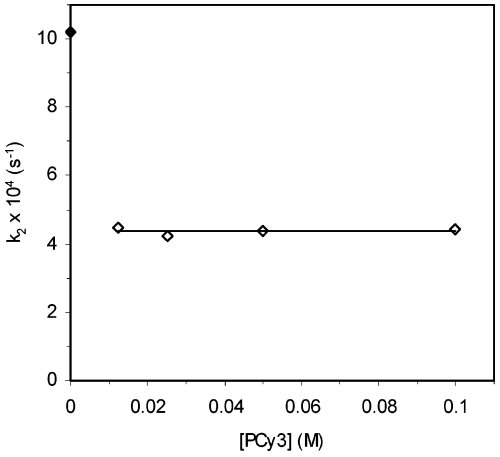

Figure 5. Graph of k_2 versus [free PCy_3] (at 62.7 °C). The curve depicts a linear least-squares fit $k_2 = a[PCy_3] + b$ ($a = 4.7 \times 10^{-5}$, $b = 4.4 \times 10^{-4}$). The filled point is provided for reference only (see Supporting Information for details) and is not included in the linear fit.

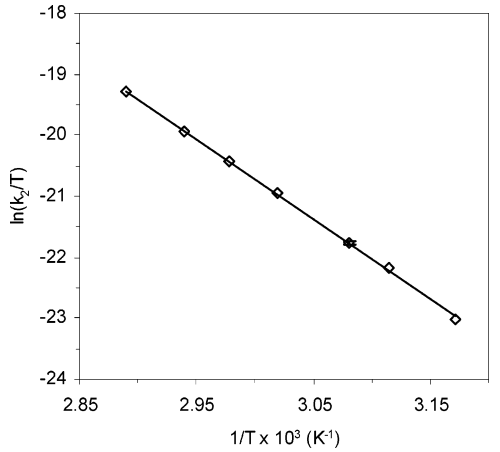

Figure 6. Eyring plot of **2** formation (k_2) in the presence of 13 mM excess PCy_3 between 42.2 and 72.9 °C. The curve depicts a linear least-squares fit to $\ln(k_2/T) = a[1/T] + b$ ($a = (-1.31 \pm 0.01) \times 10^4$, $b = 18.6 \pm 0.4$).

Between the two operative pathways, the dissociative one is the more difficult to study due to its extreme sensitivity to free PCy_3. We elected to study the nondissociative pathway instead. In subsequent studies, the dissociative pathway was effectively suppressed by the addition of a small amount of excess PCy_3 (13 mM) to all reaction solutions.[34] The deuterium kinetic isotope effect on k_2 was measured under these conditions. The observed k_H/k_D (1.8 ± 0.1) is consistent with cleavage of the C2−H bond during or prior to the rate-determining step. When the Eyring plot of k_2 was redrawn using data acquired from reactions employing excess PCy_3, a very precise linear fit was obtained ($r^2 = 0.9995$) (Figure 6). The resulting activation parameters ($\Delta H^{\ddagger} = 26.0 \pm 0.3$ kcal/mol and $\Delta S^{\ddagger} = -10.3 \pm 0.8$ cal/mol·K) reveal the dramatic extent to which metal-mediation facilitates heterocycle to NHC tautomerization.[35]

Computational Studies. In an effort to gain further insight into the microscopic steps of C−H activation, our experimental mechanistic data were augmented with DFT calculations.[36] Aided by ample structural information about **3** and **2**, a model system, using 3-methyl-3,4-dihydropyrimidine in place of **1** and PMe_3 in place of PCy_3, was constructed. After energy minimization, all bond distances common to both isolated carbene complex **2** and model carbene complex **I** differed by no more than 5%, thus ensuring the applicability of the chosen basis set and level of theory (B3LYP, LACVP**++). Starting complex **A**, the structure of which is consistent with all spectroscopic observables for **3**,[37] was connected to **I** via two possible nondissociative, intramolecular H-transfer reaction coordinates differing from one another in the manner by which they effect spatial interchange of the reacting Rh and H atoms (Figure 7).

Both pathways initially pass through transition state **B**, which involves migration of the Rh-center toward the C2−H bond and into the energy-minimized C−H σ-complex **C**. C−H σ-complexes have generally been proposed and identified along reaction coordinates for C−H activation[38] and have been specifically located along calculated pathways for the C−H oxidative addition of azoliums to $(PMe_3)_2RhCl$ and $IrH_3(PMe_3)_2$.[36] Consistent with these reports, we were readily able to locate a transition state for C−H oxidative addition (**D**) originating from the C−H σ-bound intermediate **C**. Contrary to our expectations, the resultant minimized *anti*-hydride complex (**E**) could not be connected to carbene **I**. Intramolecular H-transfer from Rh to N3 is prohibited due to the anti orientation of N and H atoms about C2−Rh bond of **E**. Nor could a transition state be located that connects **C** directly to a different hydride complex with a more favorable N−C−Rh−H dihedral angle (**G**), presumably due to improper orientation of the Rh-center with respect to the C2−H bond. Nevertheless, we were able to determine a productive reaction coordinate from *anti*-hydride complex **E** by recognizing that a 180° C−Rh bond rotation would bring N3 and the hydride into alignment for intramolecular H-transfer. A corresponding rotation transition state (**F**, 20 kcal/mol above **E**) and the desired *syn*-hydride (**G**) were successfully minimized. Finally, the transition state for H-transfer between Rh and N3 was located along the path from **G** to the final product, **I**. To our knowledge, this result constitutes the first instance of NHC formation by β-hydride insertion.

A second path to **I** was identified diverging from the "rotation" pathway at the C−H σ-complex **C**. Instead of ascending to the high-energy transition state for C−H oxidative addition, **C** was shown to undergo a low-energy Rh-migration to a second C−H σ-complex (**K**) via transition state **J**. During the migration, the Rh-center moves about the C2−H bond to a position closer N3 than N1. A transition state for oxidative addition (**L**) was located from C−H σ-complex **K**. Just as the geometry of **K** is inverse of **C**, the geometries of the resulting hydrides were also found to be inverse. Transition state **L** provides *syn*-hydride **G** directly. The remainder of the reaction

(34) Added PCy_3 does not affect the position of the preequilibrium because $(PCy_3)_2RhCl$ has been shown not to coordinate additional PCy_3 to give $(PCy_3)_3RhCl$ (ref 30b).

(35) For treatments of uncatalyzed and proton-catalyzed 1,2-hydrogen shifts at imidazol-2-yl carbenes, see: (a) Amyes, T. L.; Diver, S. T.; Richard, J. P.; Rivas, F. M.; Toth, K. *J. Am. Chem. Soc.* **2004**, *126*, 4366. (b) Bourissou, D.; Guerret, O.; Gabbai, F. P.; Bertrand, G. *Chem. Rev.* **2000**, *100*, 39.

(36) For detailed computational studies of the oxidative addition of 1,3-dimethylimidazolium to $(PR_3)_xRhCl$[36a] and $IrH_3(PMe_3)_2$,[36b] see: (a) Hawkes, K. J.; McGuinness, D. S.; Cavell, K. J.; Yates, B. F. *Dalton Trans.* **2004**, 2505. (b) Appelhans, L. N.; Zuccaccia, D.; Kovacevic, A.; Chianese, A. R.; Miecznikowski, J. R.; Macchioni, A.; Clot, E.; Eisenstein, O.; Crabtree, R. H. *J. Am. Chem. Soc.* **2005**, *127*, 16299.

(37) For the sake of simplicity, no inner-sphere solvent molecules were included in our models. In a related system, reaction coordinates calculated with inner sphere solvent did not differ significantly from coordinates lacking solvation (ref 36a).

(38) Crabtree, R. H.; Holt, E. M.; Lavin, M.; Morehouse, S. M. *Inorg. Chem.* **1985**, *24*, 1986.

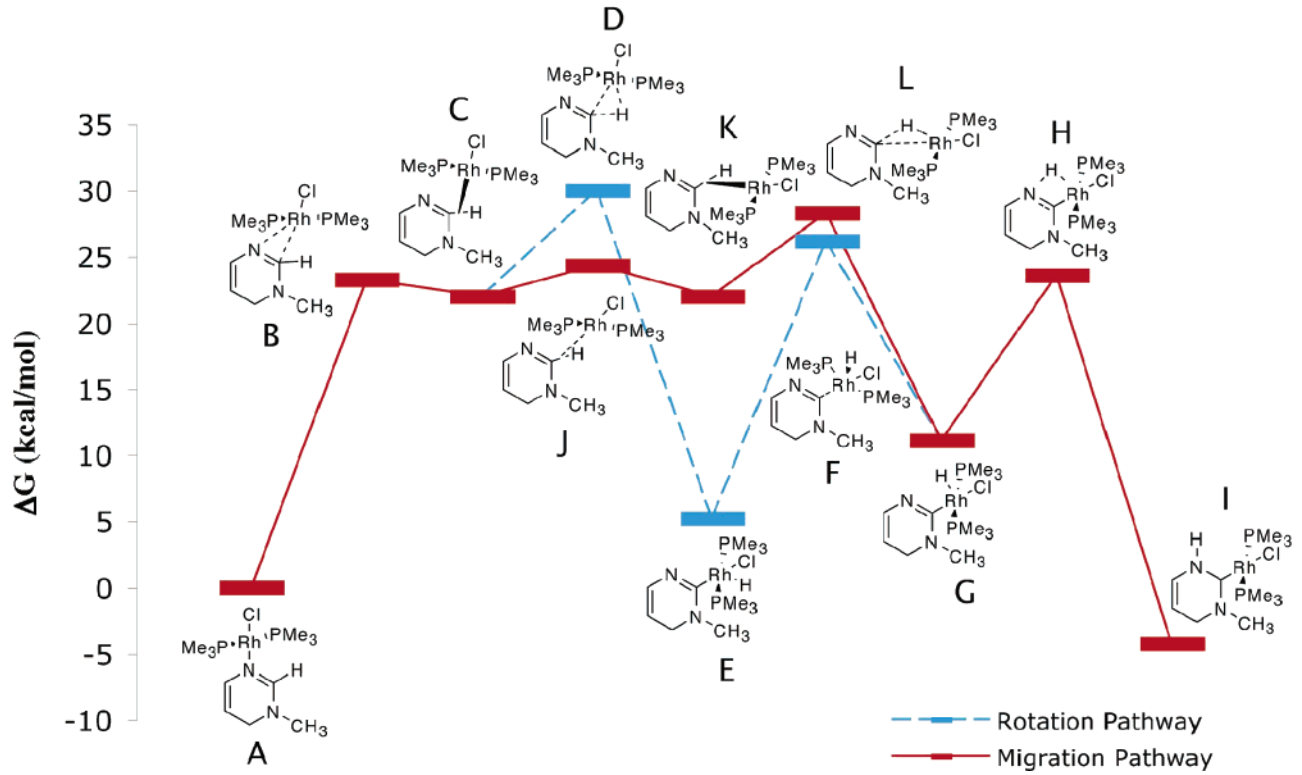

Figure 7. Calculated reaction coordinates for C−H activation (zero-point calculations, 298 K).

coordinate for the "migration" pathway is identical to that described above for the "rotation" pathway.

These mechanisms provide two possible microscopic reaction coordinates for the Rh-mediated intramolecular H-transfer leading from coordination complex **A** to NHC complex **I**. By either pathway, the computed reaction is exergonic by 4.3 kcal/mol at 298 K. This value corresponds to an equilibrium constant favoring product by $>10^3$:1, in agreement with the observation that **1** reacts irreversibly with $(PCy_3)_2RhCl$ to give **3**. Also, as in the observed reaction of **1**, neither the "migration" nor the "rotation" mechanisms predict observable intermediates other than the N1-σ-bound complex (**A**).[39] Both calculated pathways are nondissociative in phosphine and involve rate-limiting C−H activation steps, consistent with the significant primary kinetic isotope effect measured for the nondissociative pathway of **2**-formation. The activation parameters calculated for both mechanistic variants compare well with experimental values (Table 2).[40]

In the model system, the "rotation" and "migration" mechanisms seem nearly interchangeable (the highest overall barriers differ by an insignificant amount, <2 kcal/mol at 298 K). In the real system, however, when the PMe_3 ligands are replaced by considerably more bulky PCy_3 ligands, the same is not likely to be true. As a result of nonbonded interactions between the phosphine and heterocycle ligands, we expect the transition state for C2−Rh bond rotation (**F**) to be especially high in energy in the real system, possibly prohibitively so. The "migration" pathway avoids obvious steric interactions with PR_3 because the heterocycle and the Rh-square plane stay relatively perpendicular throughout the reaction coordinate. In light of this divergence, the extreme preference for bulky phosphines that we have consistently observed in Rh(I)/PR_3-catalyzed heterocycle coupling reactions can now potentially be understood in terms of the limitations that such phosphines place on accessible (deleterious) reaction pathways.

Table 2. Comparison of Measured and Computed Activation Parameters

mechanism	$\Delta G^{\ddagger}$ (kcal/mol)[a]	$\Delta H^{\ddagger}$ (kcal/mol)	$\Delta S^{\ddagger}$ (cal/mol·K)
calculated "migration"	28.3	24.0	−14.5
calculated "rotation"	30.0	26.0	−13.2
experimental[b]	29.1 ± 0.4	26.0 ± 0.3	−10.3 ± 0.8

[a] At 298.15 K. [b] Derived from Eyring plot (Figure 6).

Discussion

By combining kinetic, structural, and computational data, it is possible to draw a plausible general mechanism for the C−H activation of *N*-heterocycles by Rh(I)/PCy_3 (Scheme 6). The reaction is initiated by the association of a heterocycle to $(PCy_3)_2RhCl$ as a dative ligand through an sp^2 hybridized nitrogen. The adjacent C−H bond is then cleaved by rate-limiting intramolecular oxidative addition to give a transient rhodium hydride. A final, rapid H-transfer step restores rhodium to the +1 oxidation state, and the transformation from heterocycle to NHC is complete. Less information is available about a competing PCy_3-dissociative pathway. Because the experiment verifying the intermediacy of **3** was run under conditions in which both pathways make substantial contributions to d[**2**]/d*t*, the PCy_3-dissociative pathway can be said to proceed via intermediate **3**. Given such a ground state, the stoichiometry of

(39) While the "migration" pathway does pass through a relatively low energy rhodium−hydride intermediate (**E**), based on its relative free energy with respect to **A** (ΔG° = 5.2 kcal/mol), it is not predicted to be observable. This is consistent with the lack of observed ^{1}H NMR resonances in the hydride region.

(40) The large, negative experimental and calculated entropies of activation are similar in magnitude to that calculated for a related oxidative addition proceeding from the C−H σ-complex between 1,3-dimethylimidazolium and $(PH_3)_2RhCl$ (−10.4 cal/mol·K, ref 36a).

Scheme 6. Proposed Mechanism of C−H Activation of **1**

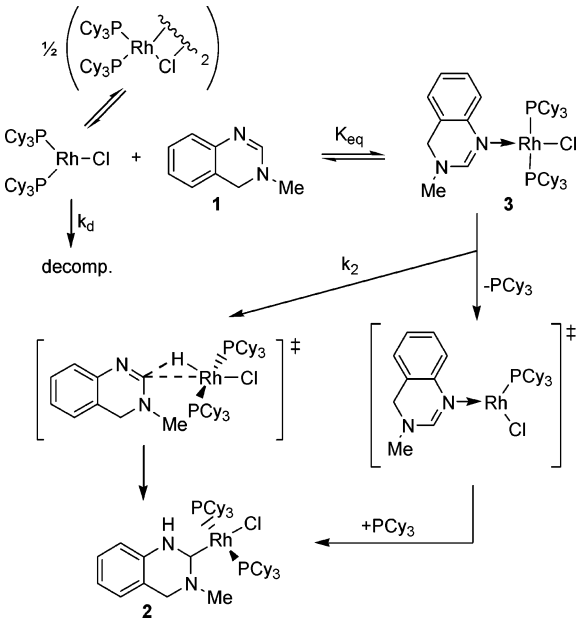

the rate-limiting transition structure is likely to be as depicted in Scheme 6. However, because the dissociative reaction could not be studied in isolation, the validity of the depicted bonding cannot be verified at this time.

This mechanism of Scheme 6 bears similarities to related directed C−H activation reactions. As in the Murai system, the directing group functions to bring the reactive metal fragment into proximity with the scissile C−H bond via pre-coordination.[41] There are substantial differences, however, between that system, which relies on a pendant directing group, and a heterocycle C−H activation system, like the one discussed here. Pendant directing groups can stay coordinated to a metal fragment during C−H oxidative addition. Often described as taking place by cyclometalation, these reaction steps are promoted by the formation of stable five- or six-membered chelate rings. Calculated models of our system, in contrast, show that the directing heteroatom (N1) must detach from the metal fragment prior to C−H cleavage.[42] Thus, catalytic functionalization of *N*-heterocycles by Rh(I)/PR$_3$ can be said to operate via a complex-induced proximity effect. Only by proceeding through an *N*-bound intermediate can the reactants gain access to an energetically accessible transition state for C−H activation.

Cavell and co-workers have recently reported a Ni^0-catalyzed C−H coupling of olefins to the 2-position of imidazolium salts (eq 7).[43] Similar to the Rh(I) C−H activation, this reaction probably proceeds through a well-characterized metal−NHC intermediate.[44] However, the proposed mechanism is most similar to that of other group 10 metal-catalyzed cross coupling reactions that operate within the M^0/M^{2+} redox couple. No experimental evidence was found for directed C−H activation via a catalyst−substrate precomplex. Despite the differences between the Rh- and Ni-based mechanisms, both seem to benefit from a well of stability along the energy surface of the catalytic cycle provided by an M−NHC intermediate. Taken together, these studies strongly contradict the notion that NHC's tend to act only as dative ligands toward transition metals.

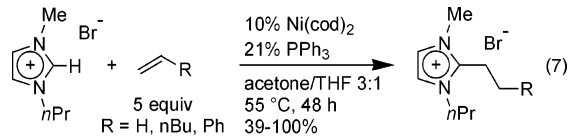

Because the Rh(I)-catalyzed functionalization reactions of dihydroquinazolines, such as **1**, occur under conditions and with selectivity patterns similar to those of the reactions of other *N*-heterocycles, the mechanism for C−H activation of **1** is likely general for Rh−NHC-mediated C−H processes. Strong predictions can thus be made about the substrate scope for Rh-catalyzed coupling reactions. Earlier work by our group showed that all competent substrates have in common the ability to form and stabilize an NHC tautomer. If our newly outlined mechanism is a general one, then it reveals the further requirement that the site of dative coordination (the sp^2-hybridized nitrogen) and the scissile C−H bond be cis to one another about a C=N double bond. Only then can facile intramolecular oxidative addition take place. All competent substrates recognized so far are cyclic and therefore meet this requirement. Potential acyclic substrates, such as formamidines or formimidates, on the other hand, are unlikely to exhibit the necessary geometry for activation, because they exist predominantly in the *S*-trans form. Indeed, in our hands, acyclic substrates have never produced coupling products. Nor have substrates requiring a hydride shift of farther than two atoms produced functionalized products to date.

The proposed reaction mechanism of Scheme 6 does provide some guidance concerning the expansion of substrate scope. Heterocycles capable of forming pyrazolyl[45] or "abnormal"-type[46] carbenes should, in principle, be compatible with this mechanism. More enticingly, our investigations reveal that the other atom (besides the sp^2-nitrogen) bonded to the carbene carbon does not directly interact with catalyst during C−H activation. While this atom may be important to the electronic structure of active substrates, our previous work has already shown that, in addition to N, the atoms S and O are tolerated at this position.[15d] Given recent reports by Bertrand and co-workers of stable amino-alkyl NHC's,[47] catalytic functionalization might now also be expected to proceed with C adjacent to the carbene position.[48] If successful, such a coupling reaction between cyclic imines and alkenes would constitute a rare example of catalytic hydroiminoacylation.[49]

(41) An instance of *ortho*-directed transition metal-mediated C−H activation that is not chelation-assisted has been recently reported: Zhang, X. W.; Kanzelberger, M.; Emge, T. J.; Goldman, A. S. *J. Am. Chem. Soc.* **2004**, *126*, 13192.
(42) Maintaining *N*-coordination during C−H oxidative addition of an *N*-heterocycle would lead to a strained three-membered chelate ring. This type of coordination is known exclusively for early metals. See ref 8 and references therein.
(43) Clement, N. D.; Cavell, K. J. *Angew. Chem., Int. Ed.* **2004**, *43*, 3845.
(44) Clement, N. D.; Cavell, K. J.; Jones, C.; Elsevier, C. J. *Angew. Chem., Int. Ed.* **2004**, *43*, 1277.
(45) Kocher, C.; Herrmann, W. A. *J. Organomet. Chem.* **1997**, *532*, 261.
(46) (a) Grundemann, S.; Kovacevic, A.; Albrecht, M.; Faller, J. W.; Crabtree, R. H. *J. Am. Chem. Soc.* **2002**, *124*, 10473. (b) Lebel, H.; Janes, M. K.; Charette, A. B.; Nolan, S. P. *J. Am. Chem. Soc.* **2004**, *126*, 5046. (c) Reference 36b.
(47) (a) Lavallo, V.; Mafhouz, J.; Canac, Y.; Donnadieu, B.; Schoeller, W. W.; Bertrand, G. *J. Am. Chem. Soc.* **2004**, *126*, 8670. (b) Lavallo, V.; Canac, Y.; Prasang, C.; Donnadieu, B.; Bertrand, G. *Angew. Chem., Int. Ed.* **2005**, *44*, 5705.
(48) We have once observed functionalization at such a site in the case of the purine (ref 15b).
(49) Efficient, versatile Rh-catalyzed hydroiminoacylation is possible when the imine *N*-substituent is a metal-coordinating group (2-pyridyl). See: Jun, C. H.; Lee, J. H. *Pure Appl. Chem.* **2004**, *76*, 577.

Conclusion

To better understand the C−H activation step governing the Rh(I)-catalyzed coupling of *N*-heterocycles and olefins, stoichiometric reactions between $(PCy_3)_2RhCl$ and heterocycle **1** were studied. The product of these reactions, a Rh−NHC complex analogous to those previously reported as catalytic intermediates (**2**), was isolated and characterized. Furthermore, a datively bound catalyst−substrate complex (**3**) was identified as an intermediate in the formation of **2**. The Rh-mediated 1,2-hydrogen shift responsible for C−H cleavage and NHC formation was studied in detail using experimental and computational methods. Based on these studies, a directed intramolecular hydrogen transfer pathway proceeding via Rh−H intermediates was implicated as the operative reaction mechanism. Similarities between the reactivity patterns of dihydroquinazolines and other *N*-heterocycles activated by $(PCy_3)_2RhCl$ suggest that this mechanism may be a common route to reactive M−NHC intermediates. Insights gained from this mechanistic study are being applied toward the ongoing development of Rh(I)-catalyzed C−H functionalization reactions in our laboratories.

Experimental Section

General. Unless otherwise noted, all reagents were obtained from commercial suppliers and degassed prior to use. Tetrahydrofuran (THF) and hexanes were passed through a column of activated alumina (A1, 12 × 32, Purifry Co.) under nitrogen pressure and sparged with nitrogen prior to use.[50] The 1,4-dioxane was purchased anhydrous, stored over 3 Å activated molecular sieves, and degassed prior to use. Benzene-d_6 was degassed by three freeze−pump−thaw cycles and stored over 3 Å activated molecular sieves. THF-d_8 was vacuum transferred from sodium/benzophenone ketyl prior to use. All compounds were stored and handled in a N_2-filled IT Braun inert atmosphere glovebox. All reactions were carried out in oven-dried glassware. Thin-layer chromatography was performed on Merck 60 F254 250-μm silica gel plates. The developed chromatograms were visualized by UV (254 nm) light. Flash column chromatography was carried out using Merck 60 230−400 mesh silica gel. All infrared (IR) spectra were recorded on a Thermo Electron Avatar 370 spectrometer fitted with a single bounce ZnSe ATR plate. Only partial IR data are listed. The ^1H, ^{13}C $\{^1H\}$, ^{31}P $\{^1H\}$, ^2H $\{^1H\}$, and ^{15}N NMR spectra were obtained on Bruker AV-300, AVQ-400, AVB-400, DRX-500, and AV-500 instruments and referenced to residual solvent. When necessary, *J* coupling was deconvoluted using ^{13}C $\{^1H, ^{15}N\}$ NMR experiments, and ^{13}C assignments were made on the basis of DEPT experiments. Elemental analyses were performed at the University of California, Berkeley, elemental analysis facility. The X-ray crystal structure was obtained at the UC Berkeley CHEXRAY. $[(coe)_2RhCl]_2$ was prepared according to literature procedures and stored at −30 °C under N_2.[51]

3-Methyl-3,4-dihydroquinazoline (1). Following a modified literature procedure,[52] 3,4-dihydroquinazoline[53] (907 mg, 6.86 mmol) and iodomethane (974 mg, 6.86 mmol) were sealed into a glass-walled vessel equipped with a vacuum stopcock with MeOH (7 mL) and allowed to stand at 25 °C for 4 d until crystallization of salts was complete. The reaction suspension was then treated with 30 mL of 0.6 M NaOH and extracted with EtOAc (3 × 30 mL). The combined organic phases were washed with brine, dried over $MgSO_4$, and concentrated onto a small amount of silica. Column chromatography on silica (5:4:0.5:0.5 EtOAc/acetone/MeOH/Et_3N) afforded a white powder that was redissolved in THF, filtered to remove traces of silica, and concentrated under vacuum. The white crystals obtained from this procedure (380 mg, 38%) exhibited spectroscopic properties consistent with literature data.[54] ^1H NMR (500 MHz, C_6D_6): δ 7.49 (d, 1H, J = 8.0 Hz, Ar−*H*), 7.07 (t, 1H, J = 7.5 Hz), 6.90 (t, 1H, J = 7.5 Hz, Ar−*H*), 6.58 (s, 1H, C2−*H*), 6.56 (d, 1H, J = 7.5 Hz, Ar−*H*), 3.74 (s, 2H, C*H*$_2$), 1.80 (s, 3H, C*H*$_3$). MS (EI); *m*/*z* (%): 145 [M^+ − H] (100), 147 [M^+ + (*D*-M^+ − H)] (47.3).

***trans*-(3-Methyl-1,2,3,4-tetrahydro-1*H*-quinazolin-2-ylidene)(P-Cy$_3$)$_2$RhCl (2, 2$_{cross}$ from Crossover Experiment).** In a N_2 atmosphere glovebox **1** (37 mg, 0.25 mmol), $[(coe)_2RhCl]_2$ (90 mg, 0.13 mmol) and PCy_3 (140 mg, 50 mmol) were combined in THF (5 mL) and sealed into a glass-walled vessel equipped with a vacuum stopcock. The reaction mixture was heated to 75 °C for 24 h and then returned to the glovebox. After the reaction solvent was removed under vacuum, **2** was obtained as a yellow solid. This material could be further purified by crystallization (slow diffusion of hexanes into THF at −30 °C under N_2) to give clear yellow blocks (153 mg, 72%). IR: 3422, 2913, 2845, 1603, 1514, 1472, 1445, 1403, 1058, 947, 732 cm^{-1}. ^1H NMR (300 MHz, d_8-THF): δ 7.99 (s, 1H, N−*H*), 7.16 (t, 1H, J = 7.6 Hz, Ar−*H*), 7.02 (d, 1H, J = 7.1 Hz, Ar−*H*), 6.92 (t, 1H, J = 7.4 Hz, Ar−*H*), 6.67 (d, 1H, J = 7.7 Hz, Ar−*H*), 4.29 (s, 2H, C*H*$_2$), 4.10 (s, 3H, C*H*$_3$), 2.3−0.9 (m, 66H, P*Cy*$_3$). ^{13}C NMR (75 MHz, d_8-THF): δ 134.4 (d, J_{Rh-C} = 1.6 Hz, *C*9), 129.5 (*C*$_{Ar}$), 127.0 (*C*$_{Ar}$), 123.5 (*C*$_{Ar}$), 118.6 (*C*10), 113.3 (*C*$_{Ar}$), 49.7 (*C*H$_2$), 48.4 (*C*H$_3$), 36.2 (t, $J_{P-C} \approx J_{Rh-C}$ = 8.2 Hz, P*C*H), 32.2 (bs, 1C, P*Cy*), 31.0 (s, 1C, P*Cy*), 29.1 (t, 2C, $J_{P-C} \approx J_{Rh-C}$ = 4.8 Hz, PCH*C*H$_2$), 28.0 (s, 1C, P*Cy*) (missing C-2 signal revealed by ^{13}C-labeling). ^{13}C NMR (100 MHz, C_6D_6) (only partial data given): δ 32.0 (P*Cy*), 30.8 (P*Cy*), 28.9 (t, $J_{P-C} \approx J_{Rh-C}$ = 4.7 Hz, PCH*C*H$_2$), 28.8 (t, $J_{P-C} \approx J_{Rh-C}$ = 4.9 Hz, PCH*C*H$_2$), 27.7 (P*Cy*). ^{31}P NMR (200 MHz, d_8-THF): δ 28.0 (d, J_{Rh-P} = 152 Hz). Anal. Calcd for $C_{45}H_{76}ClN_2P_2Rh$: C, 63.93; H, 9.06; N, 3.31. Found: C, 64.02; H, 9.14; N, 3.59. See Supporting Information for X-ray crystal structure.

***trans*-N1-(3-Methyl-3,4-dihydroquinazoline)(PCy$_3$)$_2$RhCl (3).** In a N_2 atmosphere glovebox, **1** (73 mg, 0.50 mmol), $[(coe)_2RhCl]_2$ (180 mg, 0.25 mmol), and PCy_3 (280 mg, 1.00 mmol) were dissolved in 10 mL of THF. The solution was allowed to stand for 5 d. The solid was then separated by filtration, washed with pentane, and the remaining solvent was removed under vacuum. The resulting orange powder (202 mg, 46%) was stored at −30 °C under N_2. Under these conditions, this compound is relatively stable with color change to pale green (decomposition) occurring slowly (>1 month). ^1H NMR (400 MHz, d_8-THF): δ 10.04 (d, 1H, J = 8.4 Hz, C8−*H*), 7.61 (s, 1H, C2−*H*), 7.20 (t, 1H, J = 7.6 Hz, Ar−*H*), 6.97 (t, 1H, J = 7.4 Hz, Ar−*H*), 6.71 (d, 1H, J = 7.2 Hz, Ar−*H*), 4.51 (s, 2H, C*H*$_2$), 2.97 (s, 3H, C*H*$_3$), 2.2−0.9 (m, 66H, P*Cy*$_3$). ^{31}P NMR (160 MHz, d_8-THF): δ 22.1 (d, J_{Rh-P} = 143 Hz). Inconsistent amounts of bound solvent prevented this complex from giving reliable microanalysis data.

General Procedure for the Synthesis of Isotopically Labeled 3-Methyl-3,4-dihydroquinazolines. To an NMR tube were added 2-methylaminomethyl-phenylamine (100 mg, 0.73 mmol) and 0.5 mL of formic acid. The tube was flame-sealed under vacuum and heated for 1 h until ^{13}C NMR analysis indicated that a complete reaction had occurred. After cooling, the tube contents were diluted with 2 mL of water, basified with of 0.5 mL of NH_4OH, and extracted with CH_2Cl_2 (3 × 2 mL). The combined organic phases were washed with brine, dried over $MgSO_4$, and concentrated under vacuum to give a white solid. Purification by crystallization (slow diffusion of hexanes into THF at −30 °C under N_2) gave white needles.

2-Methylaminomethyl-phenyl-^{15}N-amine (4). The reaction was run according to a modified general procedure for the amidation of aryl bromides.[55] In an N_2 atmosphere glovebox, CuI (94 mg, 0.49 mmol)

(50) Alaimo, P. J.; Peters, D. W.; Arnold, J.; Bergman, R. G. *J. Chem. Educ.* **2001**, *78*, 64.
(51) Vanderent, A.; Onderdelinden, A. L. *Inorg. Synth.* **1990**, *28*, 90.
(52) Armarego, W. L. *J. Chem. Soc.* **1961**, 2697.
(53) The 3,4-dihydroquinazoline was prepared according to a literature procedure: Lewis, J. C.; Wiedemann, S. H.; Bergman, R. G.; Ellman, J. A. *Org. Lett.* **2004**, *6*, 35.
(54) Tietz, H.; Rademacher, O.; Zahn, G. *Eur. J. Org. Chem.* **2000**, 2105.
(55) Klapars, A.; Huang, X. H.; Buchwald, S. L. *J. Am. Chem. Soc.* **2002**, *124*, 7421.

and *N*,*N*′-dimethyl-ethane-1,2-diamine (87 mg, 0.98 mmol) were combined in 1,4-dioxane (5 mL), and this mixture was stirred until the CuI completely dissolved. The resulting solution was added to a glass-walled vessel equipped with a vacuum stopcock containing (2-bromobenzyl)-methyl-amine[56] (983 mg, 4.91 mmol), ^{15}N-benzamide (600 mg, 4.91 mmol), K_2CO_3 (1.36 g, 9.83 mmol), and a magnetic stirbar. The reaction vessel was sealed and heated at 110 °C for 5.5 h until TLC (5% Et_3N in EtOAc) indicated complete consumption of the aryl bromide. The crude reaction mixture was filtered through a pad of silica eluting with CH_2Cl_2 containing 5% of a mixture of 10% NH_4OH in MeOH to give a yellow oil. This material was suspended in 5 mL of water, and then 10 mL of concentrated HCl was added dropwise. The resulting solution was washed (3 × 2 mL of Et_2O) and then resealed into the original reaction vessel and heated at 105 °C for 24 h. After being cooled to 0 °C, the reaction solution was basified by dropwise addition of NH_4OH and extracted with Et_2O (3 × 40 mL). The combined ethereal phases were washed with brine, dried over $MgSO_4$, and concentrated under vacuum to give a yellow oil. After silica gel chromatography (50% → 95% EtOAc in hexanes with 5% Et_3N), **4** (324 mg, 48%) was obtained as a yellow oil. Its spectroscopic properties were consistent with data reported for 2-methylaminomethyl-phenyl-amine.[57] ^{1}H NMR (500 MHz, C_6D_6): 7.11 (t, 1H, J = 7.6 Hz, Ar−*H*), 6.96 (d, 1H, J = 7.3 Hz, Ar−*H*), 6.73 (t, 1H, J = 7.4 Hz, Ar−*H*), 6.43 (d, 1H, J = 7.8 Hz, Ar−*H*), 4.43 (bd, 2H, J_{N-H} = 79.0 Hz, $^{15}NH_2$), 3.47 (s, 2H, CH_2), 2.01 (s, 3H, CH_3), 0.29 (bs, 1H, N*H*). ^{13}C NMR (125 MHz, C_6D_6): 148.3 (d, J_{N-C} = 10.4 Hz, *C*−^{15}N), 130.5, 129.0, 124.4 (d, J_{N-C} = 2.0 Hz), 117.8, 116.0 (d, J_{N-C} = 1.8 Hz), 56.1 (*C*H_2), 36.1 (*C*H_3). ^{15}N {^{1}H} NMR (40 MHz, C_6D_6): 55.8.

3-Methyl-3,4-dihydro-1-^{15}*N*-quinazoline (^{15}*N*1-1). The reaction was performed as described in the general procedure using **4** (100 mg, 0.73 mmol). The white solid obtained after crystallization (55 mg, 51%) exhibited spectroscopic properties consistent with data collected for **1**. ^{1}H NMR (400 MHz, $CDCl_3$): δ 7.14 (t, 1H, J = 7.6 Hz, Ar−*H*), 7.04 (d, 1H, J = 7.9 Hz, Ar−*H*), 6.98 (t, 1H, J = 7.4 Hz, Ar−*H*), 6.96 (d, 1H, J_{N-H} = 13.1 Hz, C2−*H*), 6.83 (d, 1H, J = 7.5 Hz, Ar−*H*), 4.49 (s, 2H, CH_2), 2.88 (s, 3H, CH_3). ^{13}C NMR (100 MHz, $CDCl_3$): δ 150.3 (d, J_{N-C} = 3.0 Hz, *C*2), 141.5, 128.3 (d, J_{N-C} = 3.0 Hz), 125.5, 124.6, 124.5 (d, J_{N-C} = 8.9 Hz, *C*9), 120.0, 48.9, 39.7. ^{15}N NMR (40 MHz, $CDCl_3$): δ 203.4 (d, J_{H-N} = 13.2 Hz). MS (EI); *m*/*z* (%): 145 [^{14}*N*-M$^+$ − H] (2.0), 146 [(^{14}*N*-M$^+$) + (^{15}*N*-M$^+$ − H)] (100), 147 [(^{15}*N*-M$^+$) + (^{15}*N*,*D*-M$^+$ − H)] (45.6). Calcd: 99% ^{15}*N* by comparison to the fragmentation pattern of **1**.

3-Methyl-3,4-dihydro-1-^{15}*N*,2-^{13}*C*-quinazoline (^{15}*N*1,^{13}*C*2-1). The reaction was performed as described in the general procedure using **4** (75 mg, 0.55 mmol) with ^{13}*C*-formic acid (250 mg, 5.3 mmol). The white solid obtained after crystallization (27 mg, 33%) exhibited spectroscopic properties consistent with data collected for ^{15}*N*1-**1**. ^{1}H NMR (400 MHz, C_6D_6): δ 7.49 (d, 1H, J = 7.8 Hz, Ar−*H*), 7.08 (t, 1H, J = 7.7 Hz, Ar−*H*), 6.90 (t, 1H, J = 7.4 Hz, Ar−*H*), 6.59 (dd, 1H, J_{C-H} = 190 Hz, J_{N-H} = 13.4 Hz, C2−*H*), 6.57 (d, 1H, J = 7.6 Hz, Ar−*H*), 3.75 (s, 2H, CH_2), 1.81 (d, 3H, J_{C-H} = 4.0 Hz, CH_3). ^{13}C NMR (100 MHz, THF) (only partial data given): δ 150.1 (d, J_{N-C} = 3.0 Hz, *C*2). MS (EI); *m*/*z* (%): 146 [singly labeled-M$^+$ − H] (3.2), 147 [(singly labeled-M$^+$) + (^{15}*N*,^{13}*C*-M$^+$ − H)] (100), 148 [(^{15}*N*,^{13}*C*-M$^+$) + (^{15}*N*,^{13}*C*,*D*-M$^+$ − H)] (44.8). Calcd: 96% ^{15}*N*,^{13}*C* by comparison to the fragmentation pattern of **1**.

3-Methyl-3,4-dihydro-2-^{2}*H*-quinazoline (*C*2-*D*-1). The reaction was performed as described in the general procedure using 2-methylaminomethyl-phenyl-^{14}*N*-amine[58] (125 mg, 0.92 mmol) with D_2-formic acid (500 mg, 10.4 mmol). The white solid obtained after crystallization (48 mg, 35%) exhibited spectroscopic properties consistent with data collected for **1**, except that the ^{1}H NMR signal at δ 6.6 ppm was absent, as expected. IR: 2240 cm^{-1} (C−D). ^{1}H NMR (400 MHz, C_6D_6): δ 7.51 (d, 1H, J = 7.8 Hz, Ar−*H*), 7.08 (t, 1H, J = 8.3 Hz, Ar−*H*), 6.89 (t, 1H, J = 7.4 Hz, Ar−*H*), 6.56 (d, 1H, J = 7.5 Hz, Ar−*H*), 3.74 (s, 2H, CH_2), 1.79 (s, 3H, CH_3). ^{13}C NMR (125 MHz, DCO_2D): δ 147.4 (t, J_{D-C} = 31 Hz, *C*2), 127.4, 126.9, 125.8, 124.8, 115.0, 114.9, 46.6, 39.8. ^{2}H NMR (61 MHz, C_6H_6): δ 6.6. MS (ESI); *m*/*z* (%): 147 [^{1}*H*-M$^+$ + H] (0.92), 148 [M$^+$ + H] (100), 149 [*D*-M$^+$ + H] (10.5). Calcd: 99% ^{2}*H*.

General Procedure for Observing Isotopically Labeled Rh-Complexes. To an NMR tube was added a solution containing labeled-**1** (3.8 mg, 25 μmol), $[(coe)_2RhCl]_2$ (9.0 mg, 13 μmol), and PCy_3 (14.0 mg, 50 μmol) in d_8-THF (0.5 mL). The tube was flame-sealed under vacuum, and then heated between 45 and 75 °C for 1−24 h to observe varying ratios of free **1**, **3**, and **2**. The distinctive resonances corresponding to the various complexes are reported as part of these mixtures.

From ^{15}*N*1-1: *trans*-(3-Methyl-1,2,3,4-tetrahydro-1-^{15}*NH*-quinazolin-2-ylidene)(PCy_3)$_2$RhCl (^{15}*N*1-2, 2$_{dir}$ from Crossover Experiment). Its spectroscopic properties were consistent with data collected for **2**. ^{1}H NMR (400 MHz, d_8-THF): δ 7.98 (d, 1H, J_{N-H} = 94.0 Hz, N−*H*). This compound was not sufficiently soluble to obtain an ^{15}N NMR spectrum.

***trans*-N1-(3-Methyl-3,4-dihydro-1-^{15}*N*-quinazoline)(PCy_3)$_2$RhCl (^{15}*N*1-3).** Its spectroscopic properties were consistent with data collected for **3**. ^{1}H NMR (400 MHz, d_8-THF): δ 7.61 (d, 1H, J_{N-H} = 7.2 Hz, C2−*H*). ^{31}P NMR (160 MHz, d_8-THF): δ 22.1 (d, J_{Rh-P} = 143 Hz, J_{N-P} = 3.0 Hz). This compound was not sufficiently soluble to obtain an ^{15}N NMR spectrum.

From ^{15}*N*1,^{13}*C*2-1: *trans*-(3-Methyl-1,2,3,4-tetrahydro-1-^{15}*NH*,2-^{13}*C*-quinazolin-2-ylidene)(PCy_3)$_2$RhCl (^{15}*N*1,^{13}*C*2-2). Its spectroscopic properties were consistent with data collected for ^{15}*N*1-**2**. ^{1}H NMR (500 MHz, d_8-THF): δ 7.99 (dd, 1H, J_{N-H} = 94.5 Hz, J_{C-H} = 3.9 Hz, N−*H*), 4.09 (d, 3H, J_{C-H} = 4.0 Hz, CH_3). ^{13}C NMR (125 MHz, d_8-THF): δ 216.4 (dtd, J_{Rh-C} = 54.4 Hz, J_{P-C} = 12.1 Hz, J_{N-C} = 2.0 Hz, *C*2).

***trans*-N1-(3-Methyl-3,4-dihydro-1-^{15}*N*,2-^{13}*C*-quinazoline)(PCy_3)$_2$-RhCl (^{15}*N*1,^{13}*C*2-3).** Its spectroscopic properties were consistent with data collected for ^{15}*N*1-**3**. ^{1}H NMR (500 MHz, d_8-THF): δ 7.60 (dd, 1H, J_{C-H} = 193 Hz, J_{N-H} = 7.4 Hz, C2−*H*), 2.97 (d, 3H, J_{C-H} = 4.1 Hz, CH_3). ^{13}C NMR (125 MHz, d_8-THF): δ 155.2 (d, J_{N-C} = 10.5 Hz, *C*2).

From *C*2-*D*-1: *trans*-(3-Methyl-1,2,3,4-tetrahydro-1*H*,2-^{2}*H*-quinazolin-2-ylidene)-(PCy_3)$_2$RhCl (*C*2-*D*-2, 2$_{dir,D}$ from Crossover Experiment). Its spectroscopic properties were consistent with data collected for **2**, except that the ^{1}H NMR signal at δ 8.0 ppm (N−*H*) was greatly diminished, as expected. IR: 2543 cm^{-1} (N−D).

***trans*-N1-(3-Methyl-3,4-dihydro-2-^{2}*H*-quinazoline)(PCy_3)$_2$RhCl (*C*2-*D*-3).** Its spectroscopic properties were consistent with data collected for **3**, except that the ^{1}H NMR signal at δ 7.6 ppm (C2−*H*) was absent, as expected.

Procedure for Deuterium Tracer Experiment. In a N_2 atmosphere glovebox, *C*2-*D*-**1** (3.8 mg, 26 μmol), $[(coe)_2RhCl]_2$ (8.9 mg, 12 μmol), PCy_3 (14.4 mg, 51 μmol), and 2,6-dimethoxytoluene (1.1 mg, 7 μmol) were combined in d_8-THF (0.5 mL). This mixture was flame-sealed into a medium-walled NMR tube and then heated at 70 °C overnight. After the mixture was cooled to room temperature, analysis of the reaction mixture by ^{1}H NMR indicated 80% yield of **3** with 88% incorporation of deuterium at the N1−H position.

Procedure for Double Labeling Crossover Experiment (with *C*2-*D*-1 and ^{15}*N*1-1). In a N_2 atmosphere glovebox, *C*2-*D*-**1** (0.9 mg, 6 μmol), ^{15}*N*1-**1** (0.9 mg, 6 μmol), $[(coe)_2RhCl]_2$ (4.5 mg, 6 μmol), PCy_3 (8.8 mg, 31 μmol), and 2,6-dimethoxytoluene (1.9 mg, 12 μmol) were combined in d_8-THF (0.5 mL). This mixture was flame-sealed into a medium-walled NMR tube that was then heated at 45 °C for 1 d. Periodically, the reaction tube was removed from its heating bath, cooled to room temperature, and a one-pulse ^{1}H NMR spectrum was acquired

(56) Analytical data and a synthetic protocol have been reported for (2-bromobenzyl)-methyl-amine: Philippe, N.; Denivet, F.; Vasse, J.-L.; Santos, J. S. O.; Levacher, V.; Dupas, G. *Tetrahedron* **2003**, *59*, 8049.
(57) Coyne, W. E.; Cusic, J. W. *J. Med. Chem.* **1968**, *11*, 1208.
(58) Prepared according to the procedure for **4**.

prior to reheating to 45 °C. Based on these spectra, the relative abundance of the various isotopomers of **2** was determined (Table 1).

General Procedures for Measurements of Reaction Rate. The reactions were carried out in medium-walled NMR tubes flame-sealed with a solid glass rod inside to minimize solvent reflux during heating. Reaction progress was monitored by in situ NMR analysis in the temperature-controlled probe of a Bruker DRX-500 MHz spectrometer. Instrument temperature readings were verified by reference to an ethylene glycol standard. Single pulse ^{1}H NMR spectra were collected at regular intervals of at least 5 times the longest measured T_1. The peak area of methyl and methylene resonances for the dihydroquinazoline moiety was measured relative to the internal standard (2,6-dimethoxytoluene) methoxy group peak area to obtain absolute concentrations. Initially, a reaction was run to complete conversion, and the resulting concentration versus time data were satisfactorily fit to our kinetic model (vida infra) (Figure S-1a). Subsequent reactions were monitored to between 10% and 40% conversion (Figure S-1b). Concentration versus time data were fitted using the Gepasi 3.0 software package (mass action kinetics) to obtain rate constants corresponding to Scheme 3, path A. The initial concentration of free $(PCy_3)_2RhCl$ in solution was set based on the weight of added reagents because it could not be independently measured by NMR. While the actual concentration of $(PCy_3)_2RhCl$ is determined by complex equilibria (Scheme 5), for the sake of data fitting, approximating $[(PCy_3)_2RhCl]$ as the total concentration of free Rh(I) proved to be an acceptable simplification. A term for slow unimolecular decomposition of $(PCy_3)_2RhCl$ ($k_d < 6.5 \times 10^{-5}$ s^{-1}) was included in all fits.

General Methods for Preparing Reaction Solutions for Rate Studies. Method A (in Situ Generation). In an N_2 atmosphere glovebox, **1** (1.8 mg, 13 μmol), $[(coe)_2RhCl]_2$ (4.5 mg, 6 μmol), PCy_3 (8.8 mg, 31 μmol), and 2,6-dimethoxytoluene (1.9 mg, 12 μmol) were combined in d_8-THF (0.5 mL). The resulting dark red solution was transferred to an NMR tube, frozen using liquid N_2, flame-sealed under vacuum, and kept frozen until use.

Method B (Using Isolated Intermediate). In an N_2 glovebox, **3** (11 mg, 13 μmol), PCy_3 (1.8 mg, 6 μmol), and 2,6-dimethoxytoluene (1.9 mg, 12 μmol) were transferred to an NMR tube using d_8-THF (0.5 mL). After being sealed under vacuum, the reaction tube was heated with agitation using a warm water bath (45 °C) until the light orange suspension became dark red and homogeneous. The reaction tube was maintained at 45 °C until use.

Method for Measuring Deuterium Kinetic Isotope Effect. In an N_2 atmosphere glovebox, $[(coe)_2RhCl]_2$ (9.0 mg, 12 μmol), PCy_3 (17.5 mg, 62 μmol), and 2,6-dimethoxytoluene (1.9 mg, 12 μmol) were combined in d_8-THF (1 mL). This solution was divided into two portions, one of which was combined with **1** (1.8 mg, 13 μmol) while the other was combined with *C*2-*D*-**1** (1.8 mg, 13 μmol). The resulting dark red solutions were transferred to separate NMR tubes, frozen using liquid N_2, flame-sealed under vacuum, and kept frozen until use. Reaction rates were otherwise measured as usual.

Computation Methodology. The B3LYP/LACVP**++//B3LYP/LACVP** level of theory[59] with "medium" grid density as implemented in the Jaguar 4.0 quantum chemistry program package has been utilized throughout this study.[60] For N, C, Cl, P, and H, the 6-31G basis set of Pople and co-workers was used.[61] For rhodium, a Hay−Wadt small core effective core potential replaces the 28 innermost core electrons.[62] A single asterisk (*) indicates the addition of polarization functions to atoms Li through Ar; a double asterisk indicates the addition of polarization functions to atoms H through Ar. Similarly, a single plus (+) indicates the addition of diffuse functions to atoms Li through Ar; and double pluses indicate the addition of diffuse functions to atoms H through Ar. The basis set on rhodium has double ζ quality [contraction scheme {331/311/31}]. A full geometry optimization and analytical vibrational frequency calculation were performed for all simplified models. Stationary points are characterized by exactly zero imaginary vibrations; transition structures are characterized by exactly one imaginary vibration. Gibbs free energies ΔG for 298.15 K and 1 atm are based on unscaled molecular vibrations.

Acknowledgment. We thank Dr. Fred Hollander at the UCB X-ray diffraction facility for determination of the crystal structure of **2**. Dr. Jeff Pelton of the UCB structural biology NMR facility is thanked for providing assistance for multinuclear decoupling experiments. We acknowledge Dr. Katherine Durkin of the Berkeley Molecular Graphics and Computation Facility for her helpful advice on the use of Jaguar. This work was supported by NIH grant GM069559 (to J.A.E.) and by the Director and Office of Energy Research, Office of Basic Energy Sciences, Chemical Sciences Division, U.S. Department of Energy, under contract DE-AC02-05CH11231 (to R.G.B.).

Supporting Information Available: Typical plots and numerical rate data for the formation of **2**, a Van't Hoff plot for the equilibrium between **1** and **3**, tabulated energy values for **A**−**L**, and X-ray crystallographic data for **2** in CIF format. This material is available free of charge via the Internet at http://pubs.acs.org.

JA0576684

(59) (a) Becke, A. D. *J. Chem. Phys.* **1993**, *98*, 5648−5652. (b) Vosko, S. H.; Wilk, L.; Nusair, M. *Can. J. Phys.* **1980**, *58*, 1200. (c) Lee, C. T.; Yang, W. T.; Parr, R. G. *Phys. Rev. B* **1988**, *37*, 785. (d) Krishnan, R.; Binkley, J. S.; Seeger, R.; Pople, J. A. *J. Chem. Phys.* **1980**, *72*, 650.
(60) *Jaguar 4.0*, release 23; Schrodinger, Inc.: Portland, OR, 1998.
(61) Frisch, M. J.; Pople, J. A.; Binkley, J. S. *J. Chem. Phys.* **1984**, *80*, 3265.
(62) (a) Hay, P. J.; Wadt, W. R. *J. Chem. Phys.* **1985**, *82*, 270−283. (b) Hay, P. J.; Wadt, W. R. *J. Chem. Phys.* **1985**, *82*, 299.